Front. Optoelectron. 2018, 11(4): 375–384
https://doi.org/10.1007/s12200-018-0855-4

RESEARCH ARTICLE

Efficient deep red phosphorescent OLEDs using 1,2,4-thiadiazole core-based novel bipolar host with low efficiency roll-off

Runda GUO, Wenzhi ZHANG, Qing ZHANG, Xialei LV, Lei WANG (✉)

Wuhan National Laboratory for Optoelectronics, Huazhong University of Science and Technology, Wuhan 430074, China

Abstract A series of 1,2,4-thiadiazole core-based bipolar materials, 2,2'-(1,2,4-thiadiazole-3,5-diyl)bis(*N*,*N*-diphenylaniline) (*o*-TPATHZ), 3,3′-(1,2,4-thiadiazole-3,5-diyl)bis(*N*,*N*-diphenylaniline) (*m*-TPATHZ) and 4,4'-(1,2,4-thiadiazole-3,5-diyl)bis(*N*,*N*-diphenylaniline) (*p*-TPATHZ) were developed as the host matrixes for the deep red phosphorescent emitters tris(1-phenylisoqiunoline)iridium ($Ir(piq)_3$) and [bis(2-methyldibenzo-[f,h]-quinoxaline)Ir(III)(acetylacetonate)] ($Ir(MDQ)_2(acac)$). By systematic studying, we demonstrated that there are two types of charge-trapping effect within the emissive layers through adjusting the host-guest compatibility. And, it is revealed that a symmetric charge-trapping effect can contribute to realizing a stable charge-balance, which led to a mitigating efficiency roll-off at high current density. Consequently, a maximum external quantum efficiency (EQE) of 16.2% was achieved by an optimized device with *p*-TPATHZ-$Ir(piq)_3$ emissive layer. Remarkably, the EQE still remained as high as 15.7% at the high luminance of 1000 cd/m^2.

Keywords 1, 2, 4-thiadiazole core, low efficiency roll-off, deep red phosphorescent devices, symmetrical charge-trapping effect

1 Introduction

Quantum efficiency has been regarded as the most important criterion for the evaluation of organic light-emitting diodes (OLEDs) [1–4]. In comparison to the conventional fluorescent devices, the discovery of phosphorescent OLEDs is a major breakthrough. Phosphorescent materials provide an inherent approach for ~100% excitons harnessing ability with the help of strengthened spin-orbit coupling [5–7]. Nowadays, OLED and LED could complement each other with their own advantages and meet different commercial requirements [8–10]. Throughout the past decades, numerous phosphorescent OLEDs which emit light ranging from blue to red have already been discovered [11–18]. However, there are few reports on saturated deep-red ones possessing Commission International de L'Eclairage_*x* (CIE *x*)$\geqslant$0.67 with high efficiency and low efficiency roll-off simultaneously [19,20]. Such a predicament could be mainly ascribed to the fact that the non-radiative rate constant of emitter molecules tends to increase as the energy gap decrease, which therefore deteriorates the device efficiency [21,22]. Most research efforts are devoted to new phosphorescent emitter molecules design [23,24]. However, a well matched host matrix also plays a crucial role in high-performance OLEDs. First, as is well known, a so-called host-guest system by homogeneously dispersing a phosphorescent emitter into a host matrix at a proper concentration is commonly adopted in most phosphorescent OLEDs [25–27]. It is believed that this structure contributes to suppressing the undesired excitons decay pathways such as aggregation quenching, triplet-triplet annihilation (TTA), etc. Moreover, for the purpose of suppressing a backward endothermic energy transfer and achieving an efficient host → guest energy transfer, a proper triplet energy levels (E_T) of host material is also necessary. At last, the host matrix could be seriously affects the charge-balance within the emissive layers (EMLs). Bipolar host materials have gained immense interests in recent years due to their balanced charge transport abilities.

In deep red phosphorescent OLEDs, the host matrix always possesses a much larger energy gap than the guest

Received August 10, 2018; accepted September 29, 2018

E-mail: wanglei@mail.hust.edu.cn

Special Issue—Energy Optoelectronics

materials, and the latter usually constitute charge-trapping sites within EMLs. The forms of the charge-trapping sites are different in various host-guest compatibilities. The influence of the charge-trapping effect on the device quantum efficiency is unnegligible [28–33]. In our previous work, we constructed an asymmetrical charge-trapping based on two carbazole/thiadiazole hybrids [34]. The relationship between electron-trapping and device performances was investigated and we confirmed that the hole-trapping was unfavorable in all devices. However, the difference between a symmetric and an asymmetrical charge-trapping effect is still unclear. A further investigation is necessary.

In this paper, we designed and synthesized three bipolar host materials, 2,2'-(1,2,4-thiadiazole-3,5-diyl)bis(*N*,*N*-diphenylaniline) *o*-TPATHZ**,** 3,3′-(1,2,4-thiadiazole-3,5-diyl)bis(*N*,*N*-diphenylaniline) *m*-TPATHZ**,** 4,4'-(1,2,4-thiadiazole-3,5-diyl)bis(*N*,*N*-diphenylaniline) and *p*-TPATHZ, by fine-tuning the linkage mode between 1,2,4-thiadiazole and triphenylamine. Phosphorescent emitters tris(1-phenylisoqiunoline)iridium ($Ir(piq)_3$) and [bis(2-methyldibenzo-[f,h]-quinoxaline)Ir(III)(acetylacetonate)] ($Ir(MDQ)_2(acac)$) were introduced for fabricating efficient deep red OLEDs. Due to the different energy levels and energy gaps of the materials, varied charge-trapping characteristics were obtained within different EMLs. In particular, improved performance is achieved by symmetric charge-trapping effect. The maximum external quantum efficiency (EQE) in $Ir(piq)_3$-based device utilizing *p*-TPATHZ as host matrix was 16.2%. Corresponding to a maximum current efficiency and power efficiency of 13.3 cd/A and 13.6 lm/W, respectively. And the EQE remained as high as 15.7% at the high luminance of 1000 cd/m^2, with an extremely low efficiency roll-off of about 3.1%. The Commission Internationale de l'Eclairage (CIE) coordinates were (0.68, 0.32).

2 Experimental section

2.1 General procedures

The immediate compounds and target materials were confirmed by ^{1}H NMR or ^{13}C NMR spectra on a Bruker-AF301 AT 400 MHz spectrometer. Mass spectra were carried out on an Agilent (1100 LC/MSD Trap) using atmospheric pressure chemical ionization (APCI). The Fourier transform infrared (FTIR) spectra were recorded on a VERTEX 70 FTIR Spectrometer. Elemental analyses of carbon, hydrogen and nitrogen were performed on an Elementar (Vario Micro cube) analyzer. Differential scanning calorimetry (DSC) was measured under nitrogen on a PE Instruments DSC 2920 unit at a heating rate of 10° C/min from 30°C to 300°C, and the glass transition temperature (T_g) was determined from the second heating scan. Thermogravimetric analysis (TGA) was undertaken with a PerkinElmer Instruments (Pyris1 TGA). The thermal stability of the samples were determined by measuring their weight loss while heating at a rate of 10°C/min from 30°C to 700°C under a nitrogen atmosphere. The UV-Vis absorption spectra were recorded on a Shimadzu UV-VIS-NIR Spectrophotometer (UV-3600) and the photoluminescence (PL) spectra were recorded on an Edinburgh instruments (FLSP920 spectrometer). Cyclic voltammetry (CV) measurements were carried out on a computer-controlled EG&G Potentiostat/Galvanostat model 283 at room temperature with a conventional three-electrode system, which contained a Pt carbon working electrode of 2 mm in diameter, a platinum wire counter electrode and an $Ag/AgNO_3$ (0.1 mol) reference electrode. Oxidations CVs of all compounds were performed in distilled dichloromethane with 0.1 mol tetrabutylammoniumhexafluorophosphate (Bu_4NPF_6) as the supporting electrolyte. All solutions were purged with a nitrogen stream for 10 min before measurement.

2.2 Device fabrication and measurement

The material MoO_3, 4,4′-(cyclohexane-1,1-diyl)bis(*N*,*N*-di-*p*-tolylani-line) (TAPC), *N*,*N*,*N*-Tris(4-(9-carbazolyl) phenyl)amine (TCTA), 3,3′-(5′-(3-(pyridine-3-yl)phenyl)-[1,1':3′,1″-terphenyl]-3,3″-diyl) dipyridine (TPBi), LiF as well as two emitters $Ir(piq)_3$ and $Ir(MDQ)_2(acac)$ were commercially available. All the devices were fabricated upon the surface of indium-tin-oxide (ITO)-coated glass substrates, the sheet resistance of which was approximately 25 $\Omega\cdot$square^{-1}. In fabrication procedure, after sequential chemical cleaning and drying, the substrates were exposed to oxygen plasma for 5 min. Then they were loaded into a high vacuum (under a base pressure ca. 5×10^{-6} Torr) thermal evaporation chamber, followed by successive deposition at a rate of 0.9 – 1.1 Å/s. In addition, both host and guest materials were co-evaporated and the deposition rates were precisely controlled by individual quartz-crystal thickness monitors. The light-emitting areas were determined by the overlap of two electrodes as 0.09 cm^2 and all electroluminescence (EL) properties were measured by combining the Keithley 2400 Digital Source meter with the PR655 under ambient conditions.

All the reagents and solvents used for the syntheses and measurements were purchased from commercial suppliers without further purification unless other stated. The chemical structures of the compounds were confirmed by ^{1}H NMR or ^{13}C NMR spectra, elemental analysis and mass spectrometry.

2.3 Synthesis

2,2'-(1,2,4-thiadiazole-3,5-diyl)bis(*N*,*N*-diphenylaniline) (***o*-TPATHZ**): A mixture of (2-(diphenylamino) phenyl)boronic acid (1.6 g, 5.6 mmol), 3-bromo-5-chloro-1,2,4-thiadiazole (0.5 g, 2.5 mmol), $Pd(PPh_3)_4$

(0.19 g, 0.17 mmol), K_2CO_3 (2.0 mol aqueous solution, 20 mL), toluene (40 mL) and ethanol (20 mL) were stirred under nitrogen at 100°C for 12 h. After cooling to room temperature, it was extracted with CH_2Cl_2 and water. Then, the organic layer was dried over anhydrous $MgSO_4$ and the solvent was removed by vacuum distillation. The residue was further purified by column chromatography using CH_2Cl_2 and petroleum ether as the eluent to afford a white powder 1.28 g (yield: 89%). ^{1}H NMR (400 MHz, $CDCl_3$) δ[ppm]: 8.30-8.28 (d, J = 7.60 Hz, 1H), 7.76-7.74 (d, J = 7.6 Hz, 1H), 7.50-7.46 (t, J = 8.0 Hz, 1H), 7.43-7.39 (t, J = 8.0 Hz, 1H), 7.36-7.32 (t, J = 7.2 Hz, 1H), 7.29-7.15 (m, 8 H), 7.02-6.92 (m, 13H), 6.77-6.74 (t, J = 6.8 Hz, 2H); ^{13}C NMR (100 MHz, $CDCl_3$) δ[ppm]: 180.62, 169.99, 147.64, 146.67, 146.25, 145.98, 132.56, 131.68, 131.60, 131.19, 130.78, 130.40, 129.40, 129.37, 129.03, 128.57, 127.25, 124.97, 123.14, 122.58, 122.14, 121.47; MS (APCI): calcd for $C_{38}H_{28}N_4S$: 572.2035; found: 572.2099 [M + H] +; Elemental analysis (%): calcd for $C_{38}H_{28}N_4S$: C 79.69, H 4.93, N 9.78, S 5.60; found: C 80.01, H 4.87, N 9.78, S 5.34.

3,3′-(1,2,4-thiadiazole-3,5-diyl)bis(*N*,*N*-diphenylaniline) (*m*-TPATHZ): The synthesize method of *m*-TPATHZ was referred the upper procedure with a high yield of 84%. ^{1}H NMR (400 MHz, $CDCl_3$) δ[ppm]: 8.06 (s, 1H), 7.96-7.94 (d, J = 7.6 Hz, 1H), 7.68 (s, 1H), 7.56-7.55 (d, J = 7.6 Hz, 1H), 7.34-7.22 (m, 10 H), 7.19-6.99 (m, 14 H); ^{13}C NMR (100 MHz, $CDCl_3$) δ[ppm]: 187.95, 173.47, 148.82, 148.27, 147.67, 147.21, 134.02, 131.67, 130.10, 129.59, 129.47, 129.27, 126.60, 126.20, 124.59, 124.21, 123.75, 123.51, 122.90, 122.86, 121.65, 121.23; MS (APCI): calcd for $C_{38}H_{28}N_4S$: 572.2035; found: 572.2087 [M + H] +; Elemental analysis (%): calcd for $C_{38}H_{28}N_4S$: C 79.69, H 4.93, N 9.78, S 5.60; found: C 80.10, H 4.87, N 9.73, S 5.30.

Synthesis of 4,4'-(1,2,4-thiadiazole-3,5-diyl)bis(*N*,*N*-diphenylaniline) (*p*-TPATHZ): The compound *p*-TPATHZ was synthesized according to the same procedure as the *o*-TPATHZ. Yield: 80.0%. ^{1}H NMR (400 MHz, $CDCl_3$) δ[ppm]: 8.21-8.18 (d, J = 8.8 Hz, 2H), 7.85-7.83 (d, J = 8.4 Hz, 2H), 7.33-7.24 (m, 8H), 7.16-7.04 (m, 16H); ^{13}C NMR (100 MHz, $CDCl_3$) δ[ppm]: 187.21, 173.26, 151.12, 149.65, 147.26, 146.66, 129.58, 129.37, 129.32, 128.56, 126.60, 125.62, 125.07, 124.36, 123.55, 123.42, 122.26, 121.28; MS (APCI): calcd for $C_{38}H_{28}N_4S$: 572.2035; found: 572.2106 [M + H] +; Elemental analysis (%): calcd for $C_{38}H_{28}N_4S$: C 79.69, H 4.93, N 9.78, S 5.60; found: C 80.25, H 4.86, N 9.78, S 5.11.

3 Results and discussion

3.1 Synthesis

The synthetic routes and chemical structures of the three target compounds are depicted in Scheme 1. All the compounds were prepared through the palladium-catalyzed Suzuki coupling reaction in high yield [35]. The three boric acid intermediate compounds were obtained by purchasing. Additionally, another important intermediate 3-bromo-5-chloro-1,2,4-thiadiazole was prepared according to our previous work [36]. The target compounds were all confirmed by ^{1}H NMR, ^{13}C NMR, elemental analysis, and mass spectrometry. These three host materials were further purified by repeated temperature-gradient vacuum sublimation.

3.2 Thermal properties

The thermal stabilities of all hosts were confirmed by the DSC and TGA under nitrogen atmosphere. DSC and TGA thermograms of these compounds were shown in Fig. 1, and the detailed data were summarized in Table 1. The relatively high T_g and T_d of these hosts manifest that they could form morphologically stable films and suppress the potential for phase separation during long-time device operation [37].

3.3 Photophysical properties

As shown in Figs. 2, 3 and Table 1, basic photophysical characteristics of *o*-TPATHZ, *m*-TPATHZ, and *p*-TPATHZ were analyzed by PL measurements. The larger conjugation of molecules can result lower triplet energy level (E_T). The conjugation length was in the order of *o*-TPATHZ < *m*-TPATHZ < *p*-TPATHZ. The analogous rules accord with the previous report [38]. And then the decreasing E_Ts of 2.68 eV for *o*-TPATHZ, 2.64 eV for *m*-TPATHZ and 2.41 eV for *p*-TPATHZ were obtained according to the highest-energy vibronic sub-band of the phosphorescence

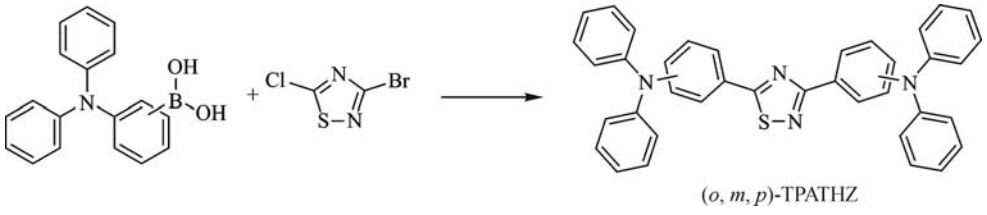

Scheme 1 Synthetic routes and chemical structures of the materials. Reaction condition: $Pd(PPh_3)_4$, K_2CO_3 (2.0 mol/L), toluene, ethanol 100°C

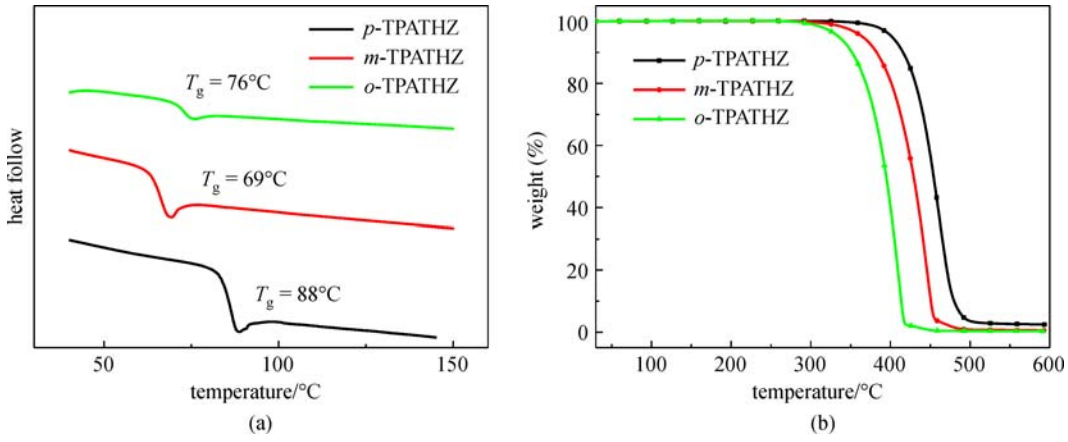

Fig. 1 (a) Differential scanning calorimetry (DSC) thermograms of *o*-TPATHZ, *m*-TPATHZ, and *p*-TPATHZ; (b) thermogravimetric analysis (TGA) curves of *o*-TPATHZ, *m*-TPATHZ, and *p*-TPATHZ recorded at a heating rate of 10°C/min

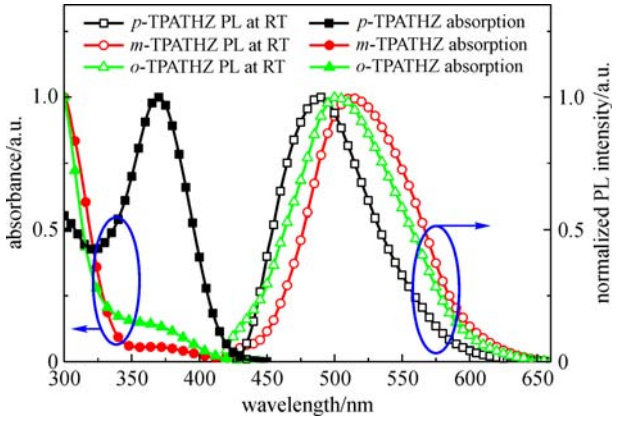

Fig. 2 Ultraviolet-visible (UV-Vis) absorption and PL spectra of *o*-TPATHZ, *m*-TPATHZ, and *p*-TPATHZ in dichloromethane (DCM). RT: room temperature

spectra. All of compounds possess a high E_T of more than 2.4 eV. It is sufficient to suppress a backward energy transfer from red phosphorescent emitters to host molecules. Noteworthy, the difference between their E_Ts is more than 0.2 eV, it provides a platform to understand the influence of E_T on triplet-triplet energy transfer efficiency.

3.4 Electrochemical properties

To investigate the highest occupied molecular orbital (HOMO) and lowest unoccupied molecular orbital (LUMO) energy levels of these hosts, oxidation scans of cyclic voltammograms were recorded as displayed in Fig. 4 and the specific data were also listed in Table 1. The HOMO levels were in the range of 5.36 to 5.41 eV, determined from the onsets of the oxidation potentials by comparing with ferrocene (F_c). Meanwhile, their LUMO levels were varied from 2.40 to 2.48 eV, determined from their band gaps (E_g) estimated from the absorption spectra. In general, all three analogs show similar HOMO and LUMO levels.

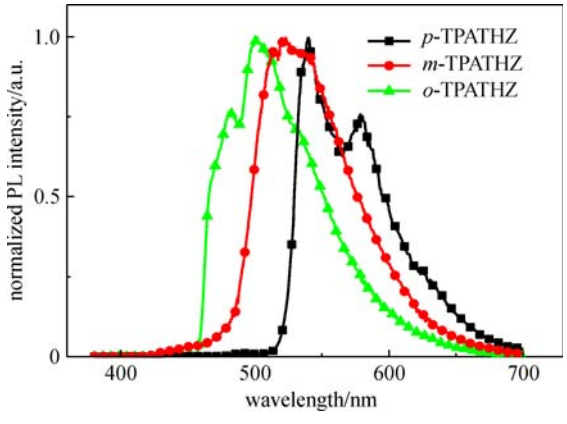

Fig. 3 PL spectra of *o*-TPATHZ, *m*-TPATHZ, and *p*-TPATHZ in 2-methyltetrahydrofuran at 77 K

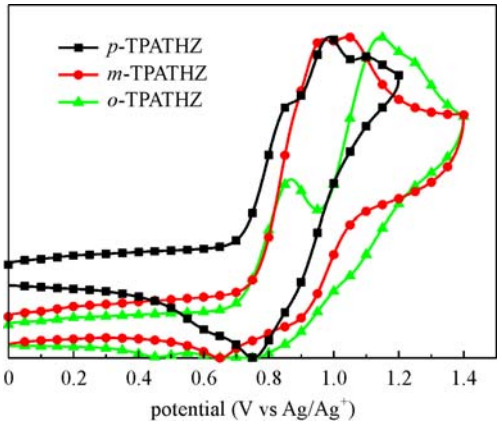

Fig. 4 Cyclic voltammograms of *o*-TPATHZ, *m*-TPATHZ, and *p*-TPATHZ at room temperature with a scan rate of 100 mV/s

Table 1 Physical properties of *o*-TPATHZ, *m*-TPATHZ, and *p*-TPATHZ

compounds	Abs[a] /nm	PL[a] /nm	T_d/T_g[b] /°C	E_g[c] /eV	E_T[d] /eV	E_{ox}[e] /V	(HOMO/ LUMO)/eV[e]	(HOMO/ LUMO)/eV[f]
o-TPATHZ	374	503	335/76	2.95	2.68	0.71	–5.36/2.41	–1.69/–4.86
m-TPATHZ	376	512	365/69	2.93	2.64	0.75	–5.41/–2.48	–1.78/–4.90
p-TPATHZ	370	490	402/88	2.97	2.41	0.71	–5.37/–2.40	–1.63/–4.86

Notes: a: Measured in CH_2Cl_2 at room temperature; b: T_d: decomposition temperatures. T_g: glass transition temperatures; c: calculated from the onset of the absorption spectra in CH_2Cl_2 solution; d: measured in 2-MeTHF glass matrix at 77 K; e: estimated from the CV; f: calculated through the density function theory (DFT)

3.5 Quantum chemical calculations

Calculated geometrical properties were investigated to figure out the influence of different substitution positions of triphenylamine (TPA) to the 1,2,4-thiadiazole (THZ) skeleton. Figure 5 shows their optimized molecular structures and orbital distribution. The HOMOs and LUMOs of *o*-TPATHZ and *m*-TPATHZ are mainly localized on the electron-rich triphenylamine (TPA) moiety and electron-withdrawing 1,2,4-thiadiazole (THZ) group, respectively. Obviously, the HOMO and LUMO are almost completely spatially separated for *p*-TPATHZ with minor electron cloud on the 1,2,4-thiadiazole (THZ) group. This separated and outside electron cloud distribution of *p*-TPATHZ can provide hole- and electron-transporting channels for intermolecular carriers hoping via their respective transporting pathways. It is in favor of improving the device performances.

3.6 Electroluminescence properties

To assess the EL performances of the novel bipolar hosts based deep red phosphorescent OLEDs, we introduced Ir $(MDQ)_2(acac)$ and $Ir(piq)_3$ as dopants. We fabricated series of devices with a typical configuration of ITO/MoO_3 (10 nm)/TAPC (40 nm)/TCTA (5 nm)/Host: $Ir(MDQ)_2(acac)$ or $Ir(piq)_3$ (3wt %, 20 nm)/TPBi (40 nm)/LiF (1 nm)/Al (100 nm) by sequential vapor deposition (Device fabrication and measurement shown in ESI). Note that the EMLs utilize $Ir(MDQ)_2(acac)$ as the emitter were named as 1 and that $Ir(piq)_3$ were named as 2. Then, *o*-TPATHZ-hosted devices were A1 and A2, *m*-TPATHZ-hosted devices were B1 and B2, and *p*-TPATHZ-hosted devices were C1 and C2, respectively. The HOMO/LUMO energy levels of the materials were illustrated in Fig. 6. Except for the host matrixes, the energy levels of other materials were from references [41,42].

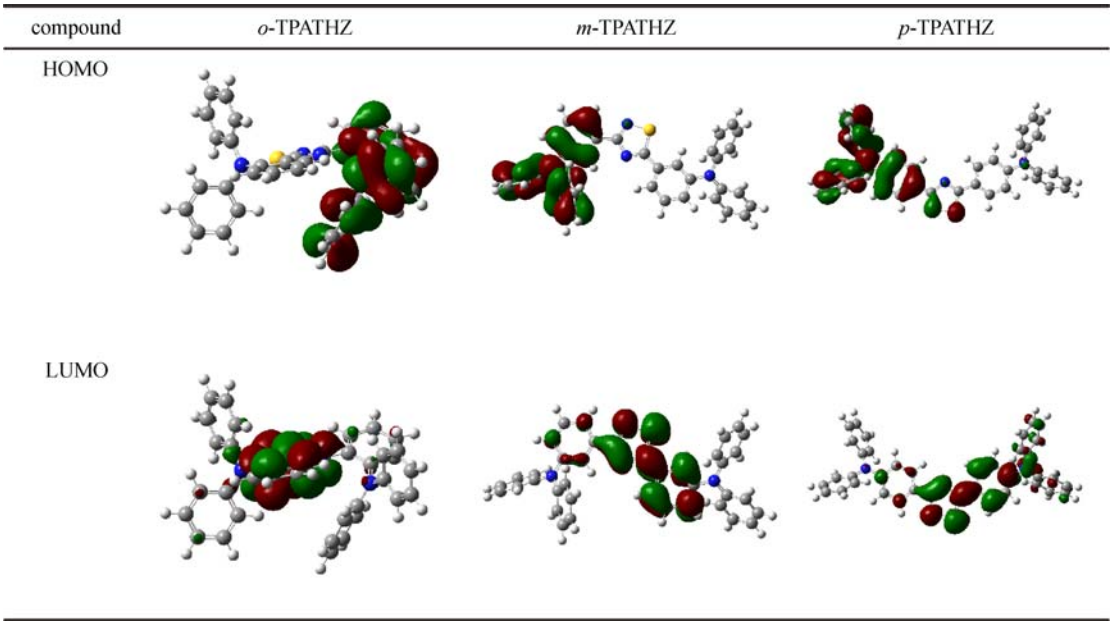

Fig. 5 Calculated HOMO/LUMO distributions and energy levels of the host materials. *Computational Details*: The geometrical and electronic properties were computed using the Gaussian 09 program package. Molecular orbitals were visualized using Gaussian view. The calculation was optimized by means of the B3LYP (Becke three parameters hybrid functional with Lee-Yang-Perdew correlation functional) [39] with the 6-31G (d) atomic basis set. Then the electronic structures were calculated at τ-HCTHhyb/6–311 + + G (d, p) level [40]. Molecular orbitals were visualized using Gaussian view

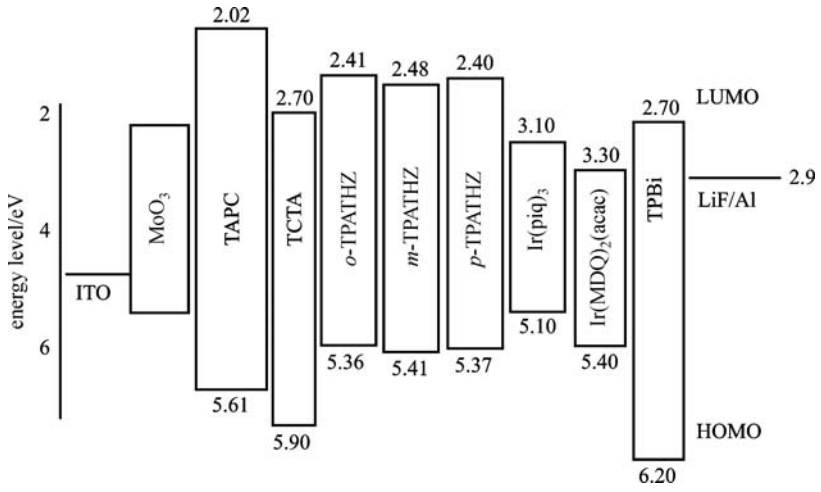

Fig. 6 Configuration of the devices based on *o*-TPATHZ, *m*-TPATHZ, and *p*-TPATHZ and the energy level diagram of all the materials used

The EQE-brightness curves were shown in Fig. 7, and the EL properties were summarized in Table 2. Although, the host-guest compatibilities are different between the two series, it is apparently that the *p*-TPATHZ-hosted devices achieved the highest EQE. For example, the maximum EQE of devices A1, B1 and C1 were 15.2%, 13.8% and 17.4%, respectively. Herein, we attributed this characteristic to their different energy transfer efficiencies, especially those governed by the Dexter mechanism process from host triplet states (T_1^H) to $Ir(MDQ)_2(acac)$ guest triplet states (T_1^G). In other words, on the basis of effectively suppressing a backward energy transfer, a relatively narrow gap between the E_T of host and that of guest could promote the $T_1^H \rightarrow T_1^G$ energy transfer.

The EQE roll-offs of the six devices were also shown in Table 2. Unlike the maximum EQE performance achieved by the two series, the efficiency roll-offs characteristic at high brightness between $Ir(MDQ)_2(acac)$-based and $Ir(piq)_3$-based devices were extremely different. As shown in Fig. 7, the roll-offs in in series 1 were much significant than those in series 2. For example, the EQE roll-off in device C1 was about 25.3% at the luminance of 100 cd/m^2, 40.8% at the luminance of 1000 cd/m^2 and as large as 71.8% at the luminance of 10000 cd/m^2, respectively. As a comparison, the EQE roll-off in device C2 was closed to zero at the luminance of 100 cd/m^2, about 3.1% at the luminance of 1000 cd/m^2 and merely 21.6% even at the luminance of 10000 cd/m^2, respectively. Furthermore, along with the sharply decreased EQE in device C1, a grown emission from *p*-TPATHZ could also be observed in its EL spectra shown in Fig. 8(a), but it's obviously vanished in Fig. 8(b). We would have a discussion about it to reveal the inner mechanism.

According to the device structure and energy level diagram shown in Fig. 6, the LUMO of $Ir(MDQ)_2(acac)$ is 3.3 eV and the LUMO of $Ir(piq)_3$ is 3.1 eV. It was obvious that the electron injection from TPBi into guest molecules was an exothermic process and the LUMO difference between the host and the guest within the EML was about 0.7 eV or even more. It means that the both two

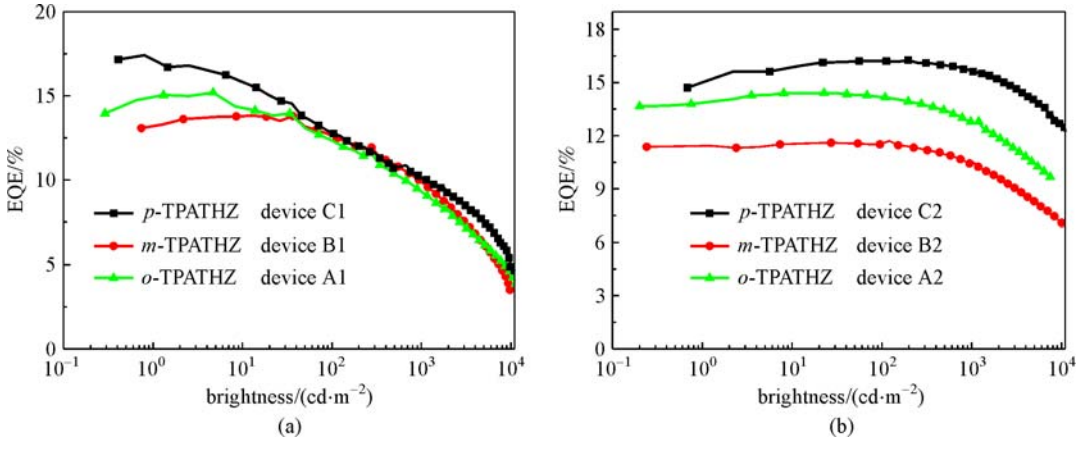

Fig. 7 EQE-brightness properties of devices (a) A1–C1 and (b) A2–C2

Table 2 EL data of devices A1–C1 and A2–C2

device	host	guest	V_{on} /V	$[\eta_c]^a$ /(cd·A^{-1})	$[\eta_p]^b$ /(lm·W^{-1})	$[\eta_{EQE}]^c$ /%	roll-off^d /%	CIE $[x, y]^e$
A1	*o*-TPATHZ	Ir(MDQ)$_2$(acac)	3.2	28.0	26.2	15.2/12.3/9.5	19.1/37.5	(0.60, 0.40)
B1	m-TPATHZ	Ir(MDQ)$_2$(acac)	3.6	24.3	19.7	13.8/12.8/10.0	7.2/27.5	(0.59, 0.39)
C1	*p*-TPATHZ	Ir(MDQ)$_2$(acac)	3.5	25.8	24.0	17.4/13.0/10.3	25.3/40.8	(0.61, 0.38)
A2	*o*-TPATHZ	Ir(piq)$_3$	3.5	11.1	10.8	14.4/14.2/12.8	1.4/11.1	(0.68, 0.32)
B2	*m*-TPATHZ	Ir(piq)$_3$	3.1	9.4	9.3	11.6/11.5/10.4	0.9/10.3	(0.67, 0.33)
C2	*p*-TPATHZ	Ir(piq)$_3$	2.9	13.3	13.6	16.2/16.2/15.7	0/3.1	(0.68, 0.32)

Notes: V_{on}: turn-on voltage; a: the maximum current efficiency; b: the maximum power efficiency; c: order of the external efficiency: maximum, at 100 and 1000 cd/m^2; d: the efficiency roll-off at 100 and 1000 cd/m^2; e: measured at 20 mA/cm^2

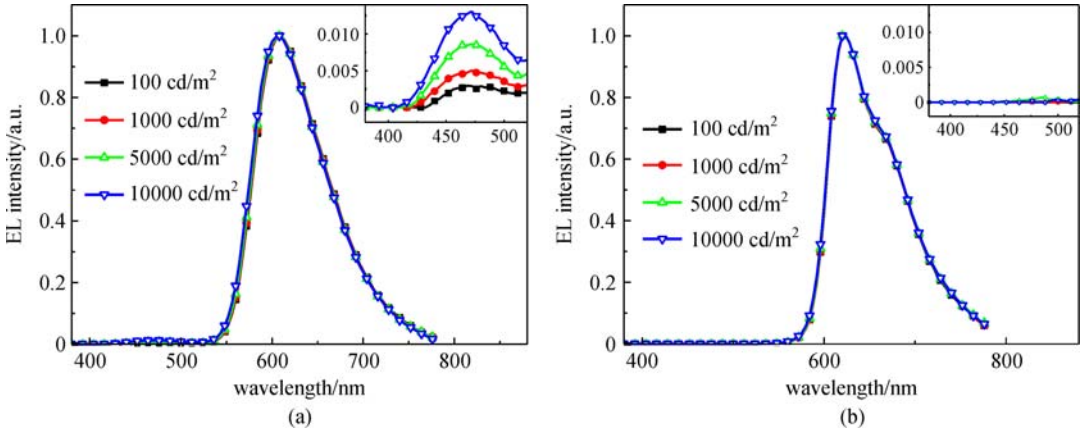

Fig. 8 EL spectra of devices (a) C1 and (b) C2. The inserts are the EL spectra when the wavelength are from 380 to 520 nm

phosphorescent emitters functioned as deep trap sites for electrons in all matrixes. In comparison, the hole-trapping effects in different devices were totally different. The HOMO of Ir(piq)$_3$ is 5.1 eV and the HOMO of Ir(MDQ)$_2$(acac) is 5.4 eV. The HOMO differences between the host materials and Ir(piq)$_3$ within the EML were about 0.3 eV while those for Ir(MDQ)$_2$(acac) is nearly zero. Due to the energy level characteristic, we assumed that the Ir(piq)$_3$ also functioned as deep hole-trapping sites in all host matrixes. That is, a symmetric and deep charge-trapping structure was constructed in Ir(piq)$_3$-based devices and stable and balance charges were maintained within the EML even though at high current density. On the contrary, an asymmetrical charge-trapping structure was constructed in Ir(MDQ)$_2$(acac)-based devices and the holes captured on Ir(MDQ)$_2$(acac) molecules can be easily de-trapped. This asymmetrical charge-trapping mode deteriorated the charge balance especially at high current density and was responsible for the significant efficiency roll-offs in devices A1, B1 and C1.

To further prove it, both hole-only devices (HODs) and electron-only devices (EODs) were introduced to estimate the charge-trapping effects in device C1 and C2. The HODs were fabricated in the structures of ITO/MoO$_3$ (8 nm)/TAPC (60 nm)/TCTA (5 nm)/*p*-TPATHZ: Ir(MDQ)$_2$(acac) or Ir(piq)$_3$ (1 wt %, 3 wt % and 6 wt %, respectively. 20 nm)/MoO$_3$ (8 nm)/Al (100 nm) and the current density-voltage (*J*-*V*) curves were shown in Fig. 9. Noteworthy, the hole-current affected by the emitter obviously in Ir(piq)$_3$-based devices but almost no change in Ir(MDQ)$_2$(acac)-based ones. Meanwhile, the EODs were fabricated in the structures of ITO/LiF (1 nm)/*p*-TPATHZ: Ir(MDQ)$_2$(acac) or Ir(piq)$_3$ (1 wt %, 3 wt % and 6 wt %, respectively. 20 nm)/TPBi (40 nm)/LiF (1 nm)/Al (100 nm). As shown in Fig. 10, deep electron-trapping effect occurred in both of Ir(MDQ)$_2$(acac) and Ir(piq)$_3$. Those observations were in accordance with the above derivations. Table 3 was given to compare the roll-offs between our works and the reported devices with Ir(piq)3. Better efficiency roll-off characteristics were achieved by utilizing our novel host materials.

4 Conclusions

We have designed and synthesized three bipolar host materials *o*-TPATHZ, *m*-TPATHZ, and *p*-TPATHZ. And we have introduced phosphorescent emitters Ir(piq)$_3$ and Ir(MDQ)$_2$(acac) to fabricate deep red OLEDs. It was found that *p*-TPATHZ-hosted devices perform best. Especially, the device incorporating both *p*-TPATHZ and Ir(piq)$_3$ has achieved a maximum EQE of 16.2% with an extremely

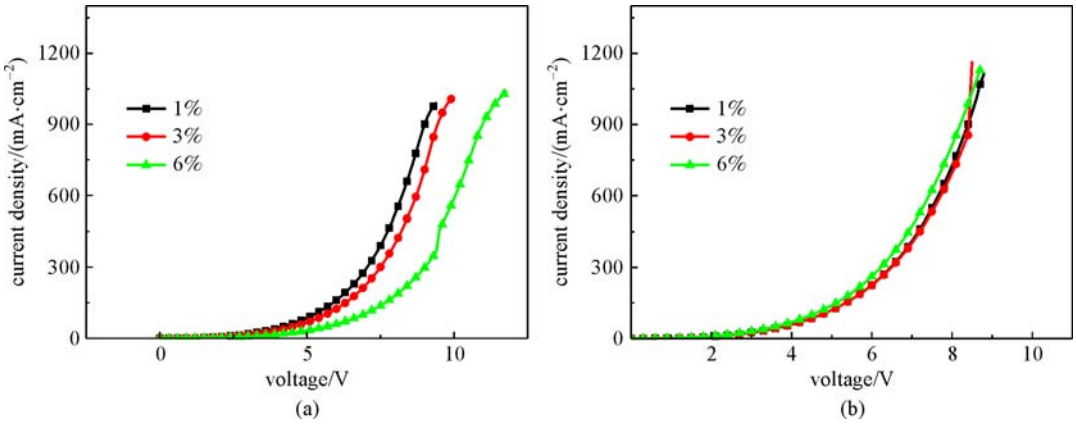

Fig. 9 Current density versus voltage curves of the hole-only devices incorporating *p*-TPATHZ and (a) $Ir(piq)_3$; (b) $Ir(MDQ)_2(acac)$

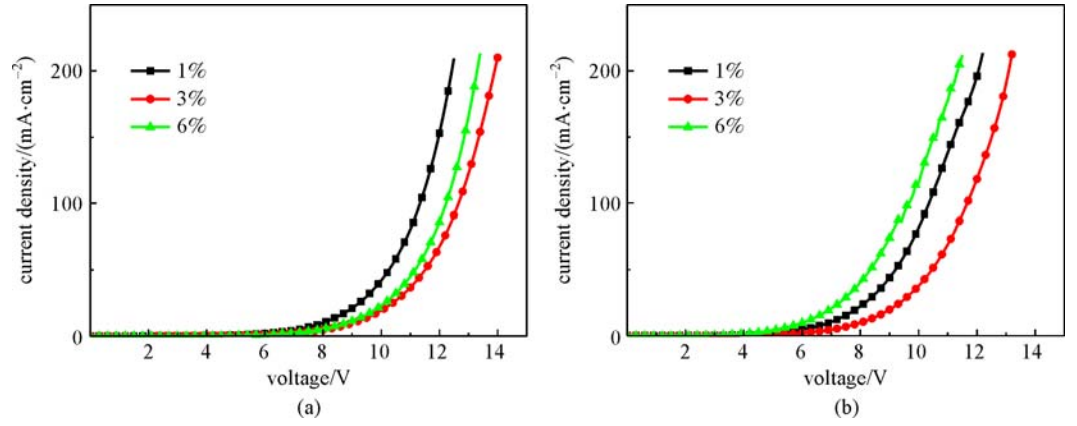

Fig. 10 Current density versus voltage curves of the electron-only devices incorporating *p*-TPATHZ and (a) $Ir(piq)_3$; (b) $Ir(MDQ)_2(acac)$

Table 3 Compare the efficiency roll-offs with reported $Ir(piq)_3$-based OLEDs

device	host	guest	$[\eta_{EQE}]^a$/%	$[\eta_{EQE}]^b$/%	roll-off^c/%
Ref. [43]	TCPB	$Ir(piq)_3$	18.6	10.2/7.93	45.2/57.4
Ref. [43]	TCPY	$Ir(piq)_3$	18.4	15.5/13.8	15.8/25
Ref. [43]	TCPM	$Ir(piq)_3$	18.2	17.8/15.4	2.2/15.4
Ref. [44]	1^d	$Ir(piq)_3$	18.2	13.6/8.36	25.3/54.1
Ref. [44]	2^d	$Ir(piq)_3$	15.8	12.6/9.9	20.3/37.3
Ref. [44]	3^d	$Ir(piq)_3$	15.7	13.2/11.6	15.9/26.1
A2	*o*-TPATHZ	$Ir(piq)_3$	14.4	14.2/12.8	1.4/11.1
B2	*m*-TPATHZ	$Ir(piq)_3$	11.6	11.5/10.4	0.9/10.3
C2	*p*-TPATHZ	$Ir(piq)_3$	16.2	16.2/15.7	0/3.1

Notes: a: the maximum EQE; b: order of the external efficiency: at 100 and 1000 cd/m^2; c: the efficiency roll-off at 100 and 1000 cd/m^2; d: synthesized novel materials reported in Ref. [44]

low efficiency roll-off of 3.1% at the luminance of 1000 cd/m^2. Deep red emission is also achieved with a CIE coordinates of (0.68, 0.32). We have also confirmed that symmetric charge-trapping effect benefit EQE roll-off characteristic through adjusting the host-guest compatibility in different devices. We indeed believed that this work will pave road to high performance deep red OLEDs.

Acknowledgements This research work was supported by the National Natural Science Foundation of China (Grant Nos. 51573065 and 51727809),

China Postdoctoral Science Foundation (No. 2017M620321), the science and technology support program of Hubei Province (No. 2015BAA075), the Fundamental Research Funds for the Central Universities, HUST (No. 2018KFYXKJC043). Thanks to SCTS/CGCL HPCC of HUST for providing computing resources and technical support. The Analytical and Testing Center at Huazhong University of Science and Technology is acknowledged for characterization of new compounds.

References

1. Forrest S R. The path to ubiquitous and low-cost organic electronic appliances on plastic. Nature, 2004, 428(6986): 911–918
2. Sasabe H, Kido J. Development of high performance OLEDs for general lighting. Journal of Materials Chemistry C, Materials for Optical and Electronic Devices, 2013, 1(9): 1699–1707
3. Reineke S, Lindner F, Schwartz G, Seidler N, Walzer K, Lüssem B, Leo K. White organic light-emitting diodes with fluorescent tube efficiency. Nature, 2009, 459(7244): 234–238
4. Xiao L, Chen Z, Qu B, Luo J, Kong S, Gong Q, Kido J. Recent progresses on materials for electrophosphorescent organic light-emitting devices. Advanced Materials, 2011, 23(8): 926–952
5. Ma Y, Zhang H, Shen J, Che C. Electroluminescence from triplet metal-ligand charge-transfer excited state of transition metal complexes. Synthetic Metals, 1998, 94(3): 245–248
6. Baldo M A, O'brien D F, You Y, Shoustikov A, Sibley S, Thompson M E, Forrest S R. Highly efficient phosphorescent emission from organic electroluminescent devices. Nature, 1998, 395(6698): 151–154
7. Yang X, Zhou G, Wong W Y. Functionalization of phosphorescent emitters and their host materials by main-group elements for phosphorescent organic light-emitting devices. Chemical Society Reviews, 2015, 44(23): 8484–8575
8. Zhuang S, Zhang W, Yang X, Wang L. A simple unilateral homogenous PhOLEDs with enhanced efficiency and reduced efficiency roll-off. Frontiers of Optoelectronics, 2013, 6(4): 435–439
9. Hussain A, Zerin T, Khan M A. Design and simulation to improve the structural efficiency of green light emission of GaN/InGaN/AlGaN light emitting diode. Frontiers of Optoelectronics, 2017, 10(4): 370–377
10. Hu X, Xia X, Zhou L, Zhang L, Wu W. Design of compensation pixel circuit with In-Zn-O thin film transistor for active-matrix organic light-emitting diode 3D display. Frontiers of Optoelectronics, 2017, 10(1): 45–50
11. Baldo M A, Lamansky S, Burrows P E, Thompson M E, Forrest S R. Very high-efficiency green organic light-emitting devices based on electrophosphorescence. Applied Physics Letters, 1999, 75(1): 4–6
12. Kim K H, Lee S, Moon C K, Kim S Y, Park Y S, Lee J H, Woo Lee J, Huh J, You Y, Kim J J. Phosphorescent dye-based supramolecules for high-efficiency organic light-emitting diodes. Nature Communications, 2014, 5(1): 4769–4777
13. Chen J, Zhao F, Ma D. Hybrid white OLEDs with fluorophors and phosphors. Materials Today, 2014, 17(4): 175–183
14. Xiang C, Koo W, So F, Sasabe H, Kido J. A systematic study on efficiency enhancements in phosphorescent green, red and blue microcavity organic light emitting devices. Light, Science & Applications, 2013, 2(6): 74–81
15. Jeon S O, Jang S E, Son H S, Lee J Y. External quantum efficiency above 20% in deep blue phosphorescent organic light-emitting diodes. Advanced Materials, 2011, 23(12): 1436–1441
16. Lee C W, Lee J Y. Above 30% external quantum efficiency in blue phosphorescent organic light-emitting diodes using pyrido[2,3-*b*]indole derivatives as host materials. Advanced Materials, 2013, 25(38): 5450–5454
17. Adachi C, Baldo M A, Thompson M E, Forrest S R. Nearly 100% internal phosphorescence efficiency in an organic light-emitting device. Journal of Applied Physics, 2001, 90(10): 5048–5051
18. Tao Y T, Wang Q, Yang C L, Zhong C, Qin J G, Ma D G. Multifunctional triphenylamine/oxadiazole hybrid as host and exciton‐blocking material: high efficiency green phosphorescent OLEDs using easily available and common materials. Advanced Functional Materials, 2010, 20(17): 2923–2929
19. Fan C H, Sun P, Su T H, Cheng C H. Host and dopant materials for idealized deep-red organic electrophosphorescence devices. Advanced Materials, 2011, 23(26): 2981–2985
20. Jou J H, Su Y T, Hsiao M T, Yu H H, He Z K, Fu S C, Chiang C H, Chen C T, Chou C H, Shyue J J. Solution-process-feasible deep-red phosphorescent emitter. Journal of Physical Chemistry C, 2016, 120(33): 18794–18802
21. Caspar J V, Meyer T J. Application of the energy gap law to nonradiative, excited-state decay. Journal of Physical Chemistry, 1983, 87(6): 952–957
22. Kim D H, Cho N S, Oh H Y, Yang J H, Jeon W S, Park J S, Suh M C, Kwon J H. Highly efficient red phosphorescent dopants in organic light-emitting devices. Advanced Materials, 2011, 23(24): 2721–2726
23. Jiang B, Gu Y, Qin J J, Ning X W, Gong S L, Xie G H, Yang C L. Deep-red iridium (III) complexes cyclometalated by phenanthridine derivatives for highly efficient solution-processed organic light-emitting diodes. Journal of Materials Chemistry C, Materials for Optical and Electronic Devices, 2016, 4(16): 3492–3498
24. Cho W, Sarada G, Lee H, Song M, Gal Y S, Lee Y, Jin S H. Highly efficient, conventional and flexible deep-red phosphorescent OLEDs using ambipolar thiophene/selenophene-phenylquinoline ligand-based Ir(III) complexes. Dyes and Pigments, 2017, 136: 390–397
25. Cheng S H, Hung W Y, Cheng M H, Chen H F, Lee G H, Chung C L, Yeh T C, Tang W C, Huang S L, Wong K T. Highly twisted carbazole-oxadiazole hybrids as universal bipolar hosts for high efficiency PhOLEDs. Advanced Electronic Materials, 2016, 2(1): 1500241
26. Wang L, Pan B, Zhu L, Wang B, Wang Y, Liu Y, Jin J, Chen J, Ma D. Construction of thermally stable 3,6-disubstituted spiro-fluorene derivatives as host materials for blue phosphorescent organic light-emitting diodes. Dyes and Pigments, 2015, 114: 222–230
27. Byeon S Y, Lee J Y. High-triplet-energy host materials derived from directly-coupled carbazole-pyridoindole moieties. Dyes and Pigments, 2016, 130: 183–190
28. Seo C W, Yoon J H, Lee J Y. Engineering of charge transport materials for universal low optimum doping concentration in phosphorescent organic light-emitting diodes. Organic Electronics, 2012, 13(2): 341–349

29. Luo Y, Aziz H. Correlation between triplet-triplet annihilation and electroluminescence efficiency in doped fluorescent organic light-emitting devices. Advanced Functional Materials, 2010, 20(8): 1285–1293
30. Kawamura Y, Brooks J, Brown J J, Sasabe H, Adachi C. Intermolecular interaction and a concentration-quenching mechanism of phosphorescent Ir(III) complexes in a solid film. Physical Review Letters, 2006, 96(1): 017404
31. Tao Y, Wang Q, Yang C, Wang Q, Zhang Z, Zou T, Qin J, Ma D. A simple carbazole/oxadiazole hybrid molecule: an excellent bipolar host for green and red phosphorescent OLEDs. Angewandte Chemie, 2008, 47(42): 8104–8107
32. Li C, Duan L, Li H Y, Qiu Y. Universal trap effect in carrier transport of disordered organic semiconductors: transition from shallow trapping to deep trapping. Journal of Physical Chemistry C, 2014, 118(20): 10651–10660
33. Li C, Duan L, Sun Y D, Li H Y, Qiu Y. Charge transport in mixed organic disorder semiconductors: trapping, scattering, and effective energetic disorder. Journal of Physical Chemistry C, 2012, 116(37): 19748–19754
34. Zhang W Z, Jin J J, Huang Z, Lv X, Zhuang S, Wang L. Towards highly efficient thermally activated delayed fluorescence devices through a trap-assisted recombination mechanism and reduced interfacial exciton annihilation. Journal of Materials Chemistry C, Materials for Optical and Electronic Devices, 2017, 5(19): 4636–4644
35. Alonso F, Beletskaya I P, Yus M. Non-conventional methodologies for transition-metal catalysed carbon–carbon coupling: a critical overview. Part 2: The Suzuki reaction. Tetrahedron, 2008, 64(14): 3047–3101
36. Jin J J, Zhang W Z, Wang B, Mu G Y, Xu P, Wang L, Huang H, Chen J S, Ma D G. Construction of high T_g bipolar host materials with balanced electron–hole mobility based on 1, 2, 4-thiadiazole for phosphorescent organic light-emitting diodes. Chemistry of Materials, 2014, 26(7): 2388–2395
37. Fan C, Chen Y, Liu Z, Jiang Z, Zhong C, Ma D, Qin J, Yang C. Tetraphenylsilane derivatives spiro-annulated by triphenylamine/carbazole with enhanced HOMO energy levels and glass transition temperatures without lowering triplet energy: host materials for efficient blue phosphorescent OLEDs. Journal of Materials Chemistry C, Materials for Optical and Electronic Devices, 2013, 1(3): 463–469
38. Lee D R, Choi J M, Lee C W, Lee J Y. Ideal molecular design of blue thermally activated delayed fluorescent emitter for high efficiency, small singlet–triplet energy splitting, low efficiency roll-off, and long lifetime. ACS Applied Materials & Interfaces, 2016, 8(35): 23190–23196
39. Lee C, Yang W, Parr R G. Development of the Colle-Salvetti correlation-energy formula into a functional of the electron density. Physical Review B, 1988, 37(2): 785–789
40. Boese A D, Handy N C. New exchange-correlation density functionals: the role of the kinetic-energy density. Journal of Chemical Physics, 2002, 116(22): 9559–9569
41. Chang Y L, Wang Z B, Helander M G, Qiu J, Puzzo D P, Lu Z H. Enhancing the efficiency of simplified red phosphorescent organic light emitting diodes by exciton harvesting. Organic Electronics, 2012, 13(5): 925–931
42. Jeon W S, Park T J, Kim S Y, Pode R, Jang J, Kwon J H. Ideal host and guest system in phosphorescent OLEDs. Organic Electronics, 2009, 10(2): 240–246
43. Su S J, Cai C, Kido J. Three-carbazole-armed host materials with various cores for RGB phosphorescent organic light-emitting diodes. Journal of Materials Chemistry, 2012, 22(8): 3447–3456
44. Su S J, Cai C, Kido J. RGB phosphorescent organic light-emitting diodes by using host materials with heterocyclic cores: effect of nitrogen atom orientations. Chemistry of Materials, 2011, 23(2): 274–284

Lei Wang is a professor in Wuhan National Laboratory for Optoelectronics (WNLO) in Huazhong University of Science and Technology (HUST). His research is focused on the area of organic light emitting diode (OLED) and quantum light emitting diode (QLED). More specifically, he is currently working on 1) the development of TADF material and device; 2) investigating small molecules that are able to harvest dark triplet state in OLED; 3) the development of the perovskite nanocrystal and its application in LED. He has published > 70 articles in peer reviewed international journals.